Journal of the Taiwan Institute of Chemical Engineers 63 (2016) 259–270

Contents lists available at ScienceDirect

Journal of the Taiwan Institute of Chemical Engineers

journal homepage: www.elsevier.com/locate/jtice

Influence of nanoparticles on mixed convection heat transfer in an eccentric horizontal annulus with rotating inner cylinder

Wael M. El-Maghlany [a,*], Mohamed M. Abo Elazm [b]

[a] Mechanical Engineering Department, Faculty of Engineering, Alexandria University, Egypt
[b] Mechanical Engineering Department, Arab Academy for Science and Technology and Maritime Transport, Alexandria, Egypt

ARTICLE INFO

Article history:
Received 11 December 2015
Revised 17 February 2016
Accepted 8 March 2016
Available online 29 March 2016

Keywords:
Mixed convection
Eccentric annulus
Nanofluid
CFD

ABSTRACT

Numerical investigation of mixed convection flow and heat transfer with different nanofluids inside an eccentric horizontal annulus is presented. The nanofluids include Cu, TiO_2 and Al_2O_3 nanoparticles with water as a base fluid. The inner and outer cylinders are kept at different constant temperatures with the inner at a higher magnitude than the outer. Moreover, the inner cylinder rotates to create the forced convection effect. Different scenarios are explored to clarify the effects of Richardson number, eccentricity ratio, and solid volume fraction with ranges of 0.01 (forced convection) $\leq$ Ri $\leq$ 100 (natural convection), $0 \leq \varepsilon \leq 0.9$, and $0.01 \leq \lambda \leq 0.05$, respectively. Results are accomplished with Grashof number, and radius ratio, equal to 10^4 and 2, respectively. The generated results include the average Nusselt number, streamlines, and isotherms. The numerical work is carried out using an in-house CFD code written in FORTRAN. Results are discussed and are found to be in good approval with preceding works. It is found that the effect of nanoparticles on the heat transfer enhancement is more pronounced at mixed convection (Ri = 1) and natural convection regions (Ri >1), however at forced convection region (Ri $\leq$ 0.1) the nanoparticles addition has an opposite effect.

1. Introduction

Recently, convection heat transfer between two eccentric and concentric cylinders has been the topic of many theoretical and experimental studies. This is due to its great importance in many engineering applications, such as heat exchangers, journal bearing, electrical motors and generators, thermal storage systems and cooling of electronic components. Many studies have been performed for the classical natural convection heat transfer problems in a horizontal annulus [1–8]; these studies were only for pure fluid. Yoo [9–11] studied the effect of Prandtl number on the natural convection within horizontal cylindrical annulus with different solutions methods. Also, the solution methodology of natural convection within concentric and eccentric annulus for both laminar and turbulent flow was performed [12–16]. In addition, the natural convection in horizontal cylindrical annulus employing porous media is studied [17–22] due to its importance in many industrial applications such as solar collector and energy storage systems.

Extraordinary considerable efforts to augment the rate of heat transfer in different ways have been executed by several investigations. As a pioneering idea, nanofluid has been announced [23–26], accordingly the natural convection in horizontal annulus is enhanced by the nanoparticles addition [27–30]. Abu-Nada et al. [31] studied the effect of nanoparticles addition on the natural convection of a nanofluid in a concentric annulus taking into account variable viscosity and variable thermal conductivity. Also, Matin and Pop [32] studied numerically the natural convection flow and heat transfer of Copper (Cu)–water nanofluid inside an eccentric horizontal annulus, they investigated the effects of eccentricity, radii ratio, nanoparticles volume fraction, Rayleigh number and Prandtl number on the average Nusselt number. It was found that the eccentricity has a significant effect on the heat transfer rate.

Mixed convection heat transfer in horizontal cylindrical annulus has less attention, Al-Amiri et al. [33] and Teamah [34] investigated numerically the double-diffusive mixed convection within a two-dimensional, horizontal annulus, with the rotation of the outer cylinder, they found that the heat transfer is influenced by Richardson number as well as Lewis number, Prandtl number, and the buoyancy ratio. Mozayyeni and Rahimi [35] performed numerical solution for mixed convection of fluid in the fully developed region in a horizontal concentric cylindrical annulus with different uniform wall temperatures, in addition, the outer cylinder is rotated in anticlockwise direction, and the fluid inside the annulus is subjected to a uniform magnetic field. Char et al. [36] performed numerical computations for turbulent mixed convection of air in horizontal concentric annulus between cooled outer cylinder

* Corresponding author. Tel.: +20 1004090302; fax: +20 452230646.
E-mail address: elmaghlany@alexu.edu.eg, elmaghlany@yahoo.com (W.M. El-Maghlany).

http://dx.doi.org/10.1016/j.jtice.2016.03.014
1876-1070/

Nomenclature

b	Annulus gab width,($r_o - r_i$), m.
C_P	Specific heat at constant pressure, J/kg K.
e	Eccentricity, m.
g	Acceleration of gravity, m/s^2
Gr	Thermal Grashof number.
k	Thermal conductivity, W/m K.
Nu	Average Nusselt number.
Nu_ϕ	Local Nusselt number.
p	Pressure, N/ m^2.
P	Dimensionless pressure.
Pe	Péclet number.
Pr	Prandtl number.
r	Radial coordinate.
r_i, r_o	Inner and outer radii respectively, m.
R	Dimensionless radial coordinates.
Ra	Thermal Rayleigh number.
Ri	Richardson number.
Re	Rotational Reynolds number.
Rr	Radius ratio.
T	Local temperature, K.
T_c, T_h	Temperatures at outer and inner radii respectively, K.
ΔT	Temperature difference, ($T_h - T_c$), K.
u	Radial velocity in transform rectangular domain, m/s.
v	Tangential velocity in transform rectangular domain, m/s.
v_r	Velocity in r-direction, m/s.
v_ϕ	Velocity in ϕ-direction, m/s.
Greek symbols	
α	Thermal diffusivity, m^2/s.
β	Coefficient of thermal expansion, K^{-1}.
ε	Eccentricity ratio.
ϕ	Angular coordinate.
λ	Solid volume fraction.
ν	Kinematic viscosity, m^2/s.
ω	Angular velocity, rad/s.
ρ	Density, kg/m^3.
θ	Dimensionless temperature.
Subscript	
f	Fluid.
nf	Nanofluid
s	Solid.

and heated, rotating inner cylinder at low Reynolds number. The results showed that the rotation has caused a significant reduction in the mean heat transfer. Khanafer and Chamkha [37] investigated mixed convection in horizontal annulus filled with a uniform fluid-saturated porous medium in the presence of internal heat generation. The inner cylinder is heated while the outer cylinder is cooled. The obtained results depicted that, Richardson number plays a significant role in the heat transfer characterization within the annulus.

Nevertheless, the studies of mixed convection [33–37] have been limited to the concentric annulus, without nanoparticles addition.

Cao et al. [38] proposed a decent methodology in simulating the complex convection heat transfer phenomena, they proposed a numerical approach for dealing with irregular geometries in dissipative particle dynamics system and by which the application of dissipative particle dynamics can be extended to mimic hydrodynamics in arbitrarily complex geometries, good agreement between their proposed methodology and both the finite volume solutions and the experimental data as well as the lattice Boltzmann method.

However, to the knowledge of the authors, it is the first time which flow in an annulus has been considered with employing mixed convection heat transfer utilizing nanofluid. The eccentricity effect on the mixed convection heat transfer in an annulus utilizing nanofluid gives a value to this study.

2. Scope and objective

The scope of the present work is focused on studying the effects of nanoparticles type (thermal properties effect) and volume fraction, on the heat transfer in an eccentric annulus subjected to mixed convection heat transfer. The numerical work is conducted after laborious affirmation and validation procedures, which demonstrated that the code solves the governing equations with insignificant numerical and modeling errors. The main objective of the present work is to establish the superior nanoparticle type from the commonly used nanoparticles (Cu, TiO_2, and Al_2O_3) to enhance the heat transfer within the eccentric annulus. The methodology followed to achieve these objectives, via numerical analysis using an in-house CFD code written in FORTRAN, were greatly built on a comprehensive, practical understanding of the verification and validation processes mandatory for CFD analysis.

3. Mathematical model and computational approach

The system under consideration is shown in Fig. 1 in both dimensional and dimensionless forms. The dimensionless form, include both polar (R,ϕ) coordinates and transform rectangular (ζ, η) coordinates. The steady-state two-dimensional mixed convection of a different nanofluid in annuli of eccentric horizontal cylinders is considered. The outer cylinder is kept cooled at temperature T_c while the inner cylinder is kept at hot temperature T_h. The eccentricity is considered below the center of the outer cylinder (downward). The temperature gradient generates the natural convection due to the buoyancy effect that signified the Grashof number while the inner cylinder rotation generates the forced convection that signified the Reynolds number. Via the inner cylinder rotation, the Richardson number ($Ri = Gr/Re^2$) is created (the Grashof number is fixed at 10^4). The following assumptions are introduced:

- Thermal equilibrium between the base fluid and nanoparticles
- Newtonian and incompressible laminar flow

Constant thermo-physical properties are considered for the nanofluid while the Boussinesq approximation is used for the density variation in the buoyancy forces.

$$\rho = \rho_o[1 - \beta\,(T - T_c)]. \tag{1}$$

Where β is the coefficient of thermal expansion such that:

$$\beta = -\frac{1}{\rho_o}\left(\frac{\partial \rho}{\partial T}\right)_{P=C}. \tag{2}$$

The governing equations for the problem under consideration are continuity, momentum and thermal energy in two dimensions steady state. For generalization, the governing equations should be in dimensionless form by the following formulations:

$$V_r = \frac{v_r}{\omega ri}, V_\phi = \frac{v_\phi}{\omega ri}, R = \frac{r}{b}, \theta = \left(\frac{T - T_c}{T_h - T_c}\right), P = \frac{p}{\rho_{nf}(\omega ri)^2},$$
$$Rr = \frac{r_o}{r_i},\ \ \varepsilon = \frac{e}{b},\ \ \mathrm{Re} = \frac{\omega\, r_i\, b}{\nu_f}, \mathrm{Pr} = \frac{\nu_f}{\alpha_f}, Ri = \frac{Gr}{\mathrm{Re}^2},$$
$$Pe = \mathrm{Re}\ \mathrm{Pr}\ ,\ U = \frac{u}{\omega ri}\ ,\ V = \frac{v}{\omega ri}. \tag{3}$$

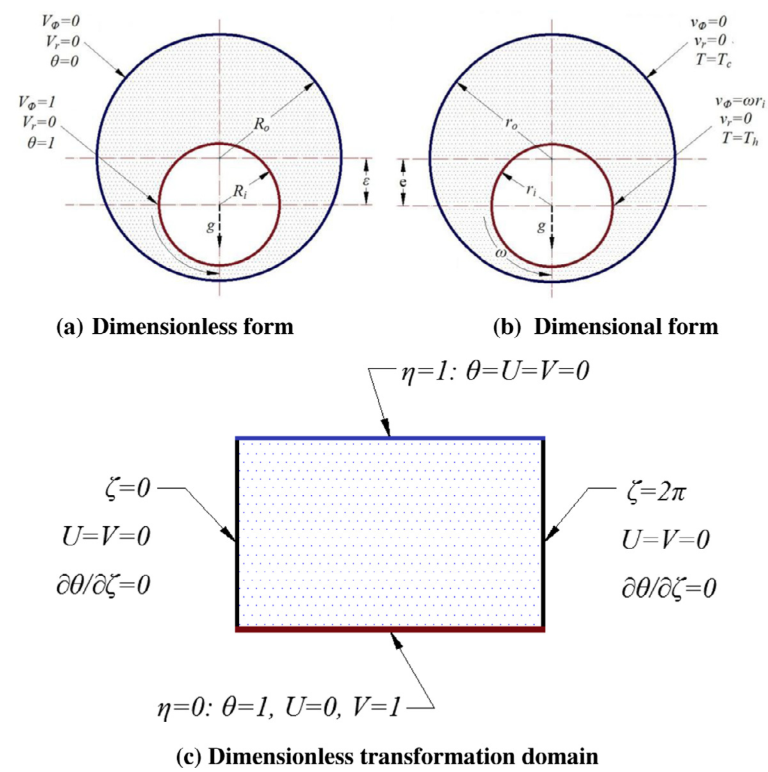

Fig. 1. Model description with boundary conditions, Rr = 2.

The dimensionless form of the governing equations of continuity, momentum and energy in cylindrical coordinate are:

$$\left(\frac{\partial V_r}{\partial R} + \frac{V_r}{R} + \frac{\partial V_\phi}{R\partial\phi}\right) = 0, \tag{4}$$

$$\left(V_r\frac{\partial V_r}{\partial R} + V_\phi\frac{\partial V_r}{R\partial\phi} - \frac{V_\phi^2}{R}\right) = -\frac{\partial P}{\partial R} - \frac{(\rho\beta)_{nf}}{\rho_{nf}\,\beta_f}Ri\,\theta\cos\phi + \frac{1}{\mathrm{Re}}\frac{\rho_f\,\mu_{nf}}{\rho_{nf}\,\mu_f}\left(\frac{\partial^2 V_r}{\partial R^2} + \frac{1}{R}\frac{\partial V_r}{\partial R} - \frac{V_r}{R^2} + \frac{\partial^2 V_r}{R^2\partial\phi^2} - \frac{2}{R^2}\frac{\partial V_\phi}{\partial\phi}\right), \tag{5}$$

$$\left(V_r\frac{\partial V_\phi}{\partial R} + V_\phi\frac{\partial V_\phi}{R\partial\phi} + \frac{V_r V_\phi}{R}\right) = -\frac{\partial P}{R\partial\phi} + \frac{(\rho\beta)_{nf}}{\rho_{nf}\,\beta_f}Ri\,\theta\sin\phi + \frac{1}{\mathrm{Re}}\frac{\rho_f\,\mu_{nf}}{\rho_{nf}\,\mu_f}\left(\frac{\partial^2 V_\phi}{\partial R^2} + \frac{1}{R}\frac{\partial V_\phi}{\partial R} - \frac{V_\phi}{R^2} + \frac{\partial^2 V_\phi}{R^2\partial\phi^2} + \frac{2}{R^2}\frac{\partial V_r}{\partial\phi}\right), \tag{6}$$

$$\left(V_r\frac{\partial\theta}{\partial R} + V_\phi\frac{\partial\theta}{R\partial\phi}\right) = \frac{k_{nf}}{k_f}\frac{(\rho\, c_p)_f}{(\rho\, c_p)_{nf}}\frac{1}{Pe}\left[\frac{1}{R}\frac{\partial}{\partial R}\left(R\frac{\partial\theta}{\partial R}\right) + \frac{\partial^2\theta}{R^2\partial\phi^2}\right]. \tag{7}$$

The dimensionless boundary conditions are:

$$V_\phi = 1, V_r = 0, \theta = 1.0, \text{at } \mathrm{R} = \mathrm{R_i}, \tag{8}$$

$$V_\phi = 0, V_r = 0, \theta = 0 \text{ and } \mathrm{C}' = 0, \text{at } \mathrm{R} = \mathrm{R_o}. \tag{9}$$

Equating the heat transfer by convection to the heat transfer by conduction at the hot wall; and introducing the dimensionless variables, defined in Eq. 3, the local Nusselt number along the inner cylinder is calculated as:

$$Nu_\phi = -\frac{k_{nf}}{k_f}\ln\left(\frac{R_o}{R_i}\right) \times \left(R\frac{\partial\theta}{\partial R}\right)_{R=Ri}. \tag{10}$$

The average Nusselt number is calculated by integrating the local value of the Nusselt number on the entire circumference of the inner cylinder as follows:

$$Nu = \frac{1}{2\pi}\int_0^{2\pi} Nu_\phi\, d\phi. \tag{11}$$

The above equations from 4 to 11 are solved for the concentric annulus ($\varepsilon = 0$). Following Lee [39], Eqs. 4–7 are transformed to a rectangular domain (η – ζ coordinates) for the eccentric annulus using the following dimensionless variables:

$\zeta = \phi$ (As the eccentricity is in the downward vertical direction),

$$\eta = \frac{R - R_b}{R_o - R_b} \text{ and } R_b = \varepsilon\cos(\zeta) + \sqrt{\varepsilon^2\cos^2(\zeta) + (R_i^2 - \varepsilon^2)}. \tag{12}$$

Accordingly, the dimensionless boundary conditions will be:

$$\begin{aligned} &\theta = 1, \quad U = 0, \quad V = 1 \;\; at \;\; \eta = 0, \\ &\theta = 0, \quad U = V = 0 \;\; at \;\; \eta = 1, \\ &\frac{\partial\theta}{\partial\zeta} = 0, \quad U = V = 0 \;\; at \;\; \zeta = 0, \\ &\frac{\partial\theta}{\partial\zeta} = 0, \quad U = V = 0 \;\; at \;\; \zeta = 2\pi. \end{aligned} \tag{13}$$

The average Nusselt number is calculated by:

$$Nu = -\frac{1}{2\pi}\frac{k_{nf}}{k_f}\int_0^{2\pi}\left(\frac{\partial\theta}{\partial\eta} \times \frac{\partial\eta}{\partial R}\right)d\zeta. \tag{14}$$

4. Numerical code details

The governing equations are solved using the finite volume method (FVM) developed by Patankar [40]. This solver, which was established in FORTRAN, was utilized by the author El-Maghlany [41–43] in several other studies, where a more detailed explanation of the solver and its validation measures were presented. The numerical solution of the momentum and the energy equations based on the finite volume method needs to convert the governing equations (momentum, energy) from the nonlinear partial differential equations system to algebraic equations system over control volume from the computational domain. The final form of the algebraic equations resulted from the discretization of the differential Eqs. 4–7 could be rewritten as:

$$a_p\Gamma_p = a_E\Gamma_E + a_W\Gamma_W + a_N\Gamma_N + a_S\Gamma_S + Q. \tag{15}$$

Eq. (15) could be rewritten as follow:

$$a_p\Gamma_p = \sum_{nb} a_{nb}\Gamma_{nb} + Q. \tag{16}$$

Γ_p : Represents the dependent variables, $\Gamma = V_r, V_\phi, \theta$.
a_P : Represents the coefficient of the variable, Γ.
a_{nb} : Represent the neighbor coefficients.
Q : This quantity resulted from the integration of the constant part of the source term.

The system of algebraic equations obtained from the discretization of the governing equations is solved iteratively (sweeping the computational domain along the radial and circumferential directions) by using the line by line procedure, and using the tridiagonal matrix algorithm (TDMA). The solving procedure is to solve simultaneously the continuity equation, momentum equations, and then the thermal energy equation.

The method of monitoring convergence is to examine how perfectly the discretization equations are satisfied by the current values of the dependent variables as recommended by Patankar [40]. For each grid point, a residual RS_Γ could be calculated from:

$$RS_\Gamma = \sum a_{nb}\Gamma_{nb} + Q - a_p\Gamma_p. \tag{17}$$

A suitable convergence criterion is to require that the largest value of $|Rs_\Gamma|$ being less than a certain small number. This small value of $|Rs_\Gamma|$ leads to that the convergence of the solution is approached when the change in the average Nusselt number through one hundred iterations, is found to be less than 0.01% of its initial value.

In order to verify the independence of the grid and the numerical results and choosing the grid of the computational domain over which the governing equations will be solved, five different mesh grids are tested, M-1 (11×6), M-2 (22×17), M-3 (45×35), M-4 (90×70) and M-5 (120×100) in R and ϕ directions (or the equivalent rectangular domain), respectively. The five meshes are verified by comparing the local and average values of Nusselt number at the different mesh sizes. Fig. 2 shows the effect of the grids number on the solution. The results indicate that there is unnoticeable difference that could be neglected between both M-4 and M-5 grids. It could be concluded that, the results obtained using the present code are independent of used grid sizes of M-4 and M-5. From this conclusion, the grid M-4 (90×70) is found to be convenient for the calculation as it gives the same results as the grid M-5 (120×100) with a significant time reduction. In order to calculate Nusselt number, the numerical differentiations, $(\frac{\partial\theta}{\partial R})_{R=R_i} = \lim_{\Delta R\to 0}(\frac{\Delta\theta}{\Delta R})$ (or equivalent rectangular domain) was performed, and the 90 grid points in R–direction are adequate to resolve the thin boundary layer near the hot inner rotating cylinder (location of Nusselt number calculation).

5. Modeling of the nanofluid thermophysical properties

The thermo-physical properties of the base fluid and the different nanoparticles are listed in Table 1. The effective density, heat capacitance, thermal diffusivity, and thermal expansion coefficient of the nanofluid are given by [43].

Table 1
Thermophysical properties of pure water and nanoparticles [43].

Physical properties	Pure water	Cu	Al_2O_3	TiO_2
ρ (kg/m^3)	997.1	8933	3970	4250
C_P (J/kg K)	4179	385	765	686.2
k (W/m K)	0.613	400	40	8.9538
β (K^{-1})	21 $\times 10^{-5}$	1.67 $\times 10^{-5}$	0.85 $\times 10^{-5}$	0.9 $\times 10^{-5}$

$$\rho_{nf} = (1-\lambda)\rho_f + \lambda\rho_s \tag{18}$$

$$(\rho C_p)_{nf} = (1-\lambda)(\rho C_p)_f + \lambda(\rho C_p)_s \tag{19}$$

$$\alpha_{nf} = k_{nf}/(\rho C_p)_{nf} \tag{20}$$

$$(\rho\beta)_{nf} = (1-\lambda)(\rho\beta)_f + \lambda(\rho\beta)_s \tag{21}$$

A number of trials exist that deal with the thermal conductivity of conventional solid–liquid mixtures. All these paid no attention to the effects of the random motion of the suspended particles and of the structure of aggregates inside the mixture. Among them, Maxwell's expression [44] is introduced to calculate the effective thermal conductivity.

$$k_{nf} = k_f\left[\frac{(k_s+2k_f) - 2\lambda(k_f-k_s)}{(k_s+2k_f)+\lambda(k_f-k_s)}\right]. \tag{22}$$

However, the random motion of the suspended nanoparticles should be considered in order to obtain a formula for the effective thermal conductivity. This formula includes the effect of the Brownian motion of the nanoparticles and is given by Koo and Kleinstreuer [45] as:

$$k_{nf} = k_f\left[\frac{(k_s+2k_f) - 2\lambda(k_f-k_s)}{(k_s+2k_f)+\lambda(k_f-k_s)}\right] + 5\times 10^4 \delta\,\lambda\,\rho_f C_{p,f}\sqrt{\frac{\kappa_b T}{\rho_s d_s}}\,f(T,\lambda). \tag{23}$$

The effective viscosity of the nanofluid containing a dilute suspension of small rigid spherical particles is given by Koo and Kleinstreuer [45] as:

$$\mu_{nf} = \frac{\mu_f}{(1-\lambda)^{2.5}} + 5\times 10^4\delta\,\lambda\,\rho_f\sqrt{\frac{\kappa_b T}{\rho_s d_s}}\,f(T,\lambda). \tag{24}$$

Both δ and $f(T,\lambda)$ could be obtained according to the nanoparticles type, the nanoparticles volume fraction and the nanoparticles diameter (d_s) [47] while κ_b represents the Boltzmann constant [44].

Fig. 3 includes the average Nusselt number variation with Richardson number, eccentricity ratio, and the nanoparticles volume fraction for the two different models to the nanofluids effective viscosity and effective thermal conductivity. One model is according to Maxwell's expression [44] and Brinkman [46] and the other that considers the effect of random motion through the nanofluid [45]. Very small differences were found between the results obtained using both models. In the present study, all results are based on the more accurate model that considers the static and random motion of the nanoparticles [45].

6. Program endorsement and comparison with preceding work

In order to check the exactness of the numerical solution method employed for the present study, it is validated against the announced results by Matin and Pop [32] for pure water

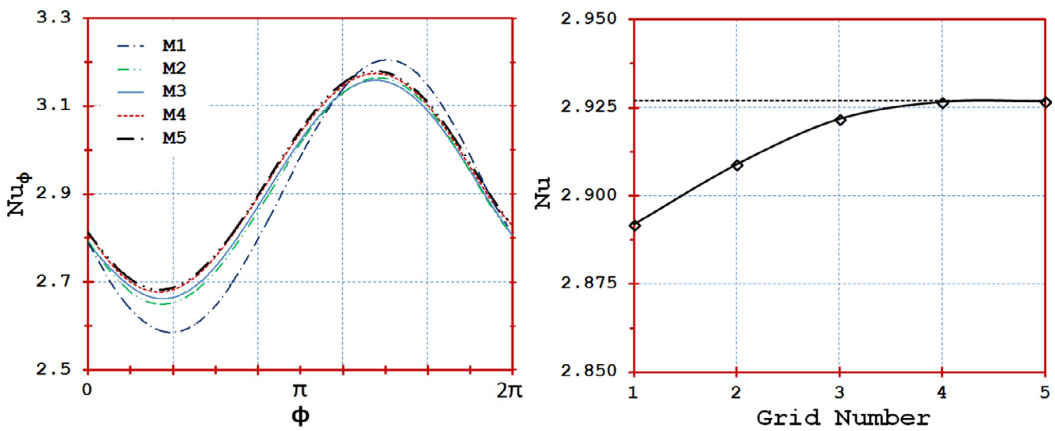

Fig. 2. Local and average Nusselt numbers at hot wall side for different grid sizing, Rr = 2, Ri = 0.01, $\lambda = 0$, $\varepsilon = 0$ and Pr = 6.2.

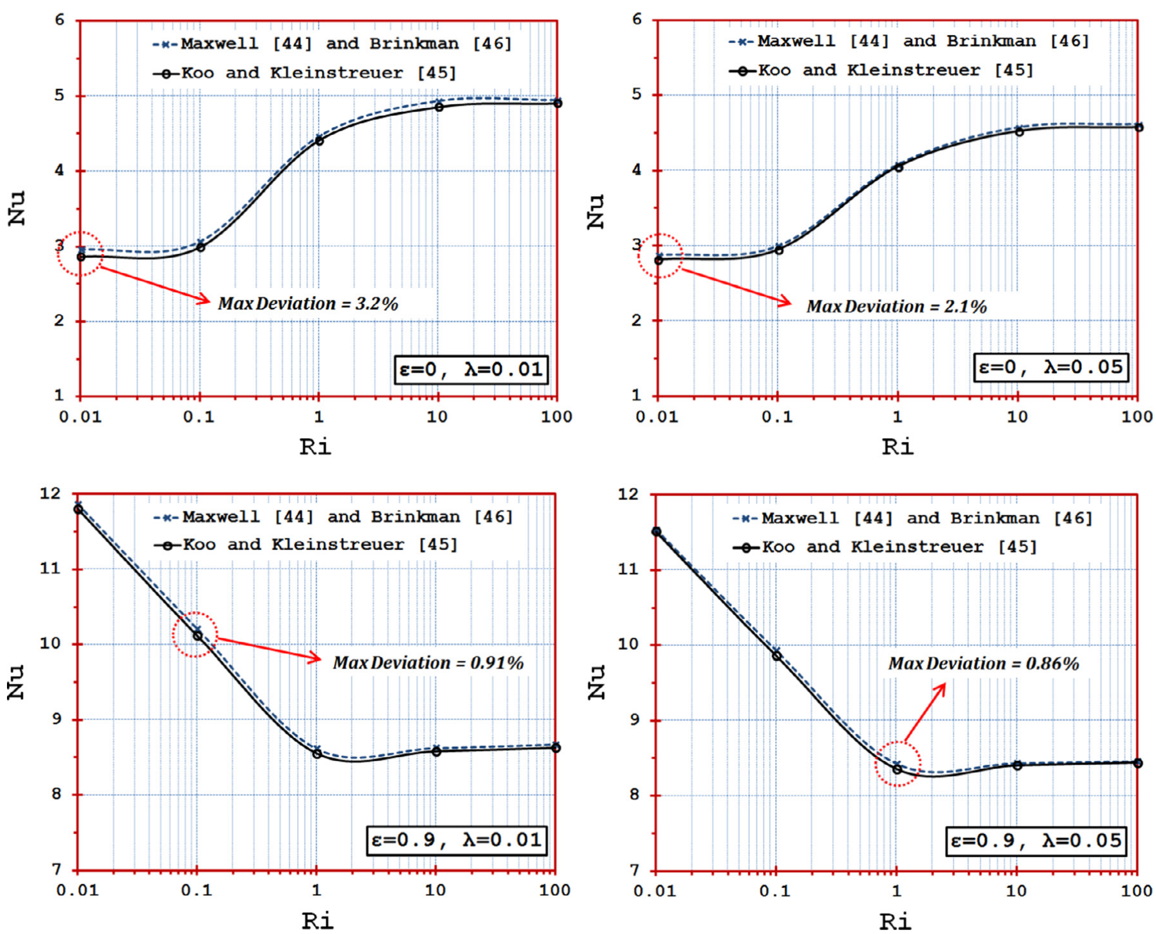

Fig. 3. Comparison between Maxwell [44] and Brinkman [46] models and Koo and Kleinstreuer [45] model on the average Nusselt number at different Richardson number with Cu–Water nanofluid.

(regular fluid) ($\lambda = 0.0$, Pr = 6.21) natural convection (Ra = 10^5) in an eccentric annulus ($\varepsilon = 0.5$ downward) for both streamlines and isotherms. Owing to the symmetry of both contours; the contours in right half are for the present code, and the contours in left half are for Matin and Pop [32], Fig. 4. Fig. 5, represents another validation of the average Nusselt number for Cu–water nanofluid ($0 \leq \lambda \leq 0.03$, Pr = 6.21) natural convection (Ra = 10^4) in a concentric annulus ($\varepsilon = 0$) and an eccentric annulus ($\varepsilon = 0.5$ downward). The figure shows a convinced approval between the present code and their results.

7. Results and discussion

In the following sections, the effects of various parameters on the considered problem are introduced. These parameters are Richardson number, eccentricity ratio, and solid volume fraction for different nanoparticles (Cu, TiO_2, and Al_2O_3). The range of Richardson number Ri, solid volume fraction of the nanoparticles λ, and the eccentricity ratio ε, are $0.01 \leq Ri \leq 100$, $0.01 \leq \lambda \leq 0.05$, and $0 \leq \varepsilon \leq 0.9$, respectively. Prandtl number Pr is set to 6.2 representing water. All results are performed with thermal Grashof

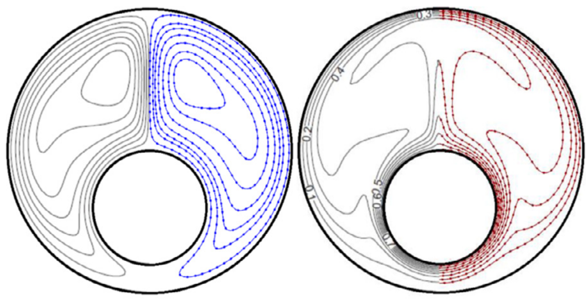

Fig. 4. Comparison between Matin and Pop (left section) [32] and present code (right section) for pure water, Rr = 2.5, Ra = 105, and $\varepsilon = 0.5$.

number Gr, and radius ratio Rr, equal to 10^4 and 2, respectively. As a base case, the pure water ($\lambda = 0$) is set as a reference to determine the enhancement in heat transfer due to the addition of nanoparticles.

7.1. Effects of Richardson number, and eccentricity ratio on the flow structure and temperature contours

The variation of the nanoparticles volume fraction (λ) on the behavior of the flow structure is related to the associated change in the nanofluid dynamic viscosity. However, the profile of the streamlines almost the same with an insignificant change due to the change in the dynamic viscosity, Fig. 6. Consequently, the nanoparticles volume fraction has been held at fixed value equals to $\lambda = 0.03$ as a sample of the obtained results. Also, the nanoparticles type (Cu, TiO_2, and Al_2O_3) effect on the flow structure has a slight effect without insignificant variation in the streamlines profile but only on their strength. This effect will be reflected in the values of the Nusselt number that will be presented later. As a sample of the case studies, the streamlines and isotherms will be discussed for TiO_2-water nanofluid with a volume fraction $\lambda = 0.03$.

The effect of the Richardson number on the streamlines is shown in Fig. 7a for concentric annulus ($\varepsilon = 0$) and eccentric annulus ($\varepsilon = 0.5$ and 0.9) with $\lambda = 0.03$ and water–TiO_2 nanofluid.

ε = 0: at Ri = 0.01, the strong effect of the inner cylinder rotation on the contact nanofluid layer is established. This effect overcomes the vertical buoyancy flow due to the natural convection effect. The inner cylinder rotational inertia is transmitted through the nanofluid layers via the viscosity effect. Owing to the uniform annulus width in the circumferential direction ($\varepsilon = 0$); the streamlines are formed as circular rings close to the rotating inner cylinder and diverge in the radial direction. As the Richardson number increases to Ri = 1, the effect of the inner cylinder rotation is limited to the contact nanofluid layers. The rest of the annulus is subjected to the buoyancy force sustained by the temperature gradient (natural convection effect); therefore, clockwise airfoil profile vortex in the right section of the annulus is formed while the left section is affected by the counter-clockwise rotation of the inner cylinder. As the Richardson number increases to Ri = 100, the effect of the inner cylinder rotation vanishes and the annulus is totally subjected to the buoyancy force sustained by the temperature gradient (natural convection effect). Consequently, a clockwise vortex in the right section of the annulus and counter-clockwise vortex in the left section are formed with an airfoil profile.

ε = 0.5: As the eccentricity ratio increases, the gap between the two cylinders increases above the inner cylinder and decreases underneath, so that natural convection is enhanced in the upper part of the annulus. At Ri = 0.01, the effect of inner cylinder rotation is signified merely at the narrow space below the inner cylinder. However, the effect of the inner cylinder rotation is lessened in the upper annulus part, and the natural convection is announced and forms a large stretched vortex above the inner cylinder. As the Richardson number increases to Ri = 1 and 100, the effect of the inner cylinder rotation is gradually damped, and the heat transfer is mainly by natural convection. Via the natural convection effect, two large vortices in opposite direction of rotation are formed with a negligible effect of the forced convection.

ε = 0.9: As the eccentricity noticeably increases, the annulus with the nanofluid is utilized above the inner cylinder *i.e.* high natural convection effect with weak forced convection effect. The streamlines profile takes the same form as $\varepsilon = 0.5$ but with more strengthen upper vortices. It should be observed that at Ri = 100 with large eccentricity ($\varepsilon = 0.9$), the flow in the annulus is regularly natural convection flow with the absence of the forced convection effect. It could be concluded that the eccentricity in the downward direction enables unrestricted fluid motion at the top of the inner cylinder that assists the natural convection effect to be noteworthy.

Fig. 7b represents the effect of both Richardson number and eccentricity ratio on the isotherms, the isotherms profile gives a complete map explains the mechanism of the heat transfer. At Ri = 100, the natural convection is dominated, and a plume above the inner cylinder is formed towards the fixed outer cylinder due to the natural convection effect at different eccentricities ($\varepsilon = 0$, 0.5, 0.9). However, the higher the eccentricity ratios, the higher the isotherms density near the hot inner cylinder ($\partial\theta/\partial R$ increased), which indicates a significant enhancement in the heat transfer. As the Richardson number decreases to 0.01, the forced convection is dominated, and the plume vanishes gradually. With $\varepsilon = 0$, the natural convection effect vanishes, and the isotherms are in logarithmic distribution characterizes a conduction heat transfer (low heat transfer rate). As the eccentricity increases to $\varepsilon = 0.9$, the density of the isotherms increases associated with an enhancement in heat transfer. If the Richardson number is unity (Ri = 1), the effect of both natural convection and forced convection is pronounced. The isotherms are in mixed convection profiles that are affected by both natural and forced convection heat transfer mechanism.

The above clarification of the isotherms will be valuable in the discussion of the desired major heat transfer parameter that is called the Nusselt number.

7.2. Effects of Richardson number, nanoparticles volume fraction, and eccentricity ratio on the average Nusselt number

The core outcome of the present study is the average Nusselt number involves the heat transfer coefficient valuation. First, as the Richardson number decreases, the heat transfer is mainly influenced by the forced convection heat transfer; this means high Nusselt number. This phenomenon compartment only on the internal forced flow (the flow inertia force). However, in a lid-driven cavity or lid-driven annulus, the influence of the externally forced convection is established at the thin fluid layer in contact with the moving part. This effect is transmitted inversely with the gap or the annulus width and proportionally with the fluid viscosity. Consequently, in this study, the heat transfer enhancement not necessarily related to the lower values of the Richardson number, but with the other parameters contribution (ε, λ, and nanoparticles physical properties). Fig. 8 represents the effect of the Richardson number, nanoparticle volume fraction, the eccentricity ratio and nanofluid constituents on the average Nusselt number. In general, the higher the eccentricity ($\varepsilon = 0.9$ downward), the higher the Nusselt number at different considered parameters (ε, λ, and nanoparticles physical properties). This could be explained as the downward movement strengthens the upward natural convection effect within the inflated space above the hot inner cylinder. The

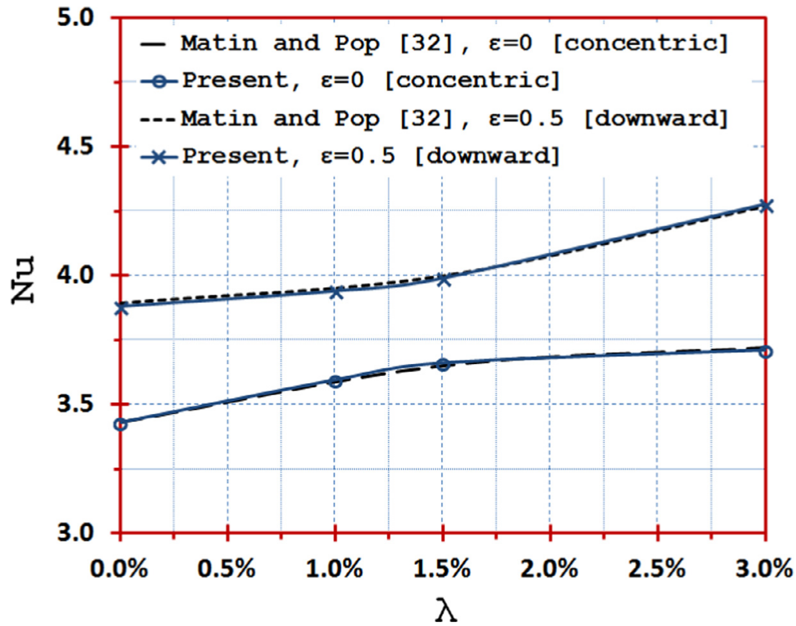

Fig. 5. Comparison between Matin and Pop [32] and the present code results for Cu–Water nanofluid, Rr = 2.5 and Ra = 104.

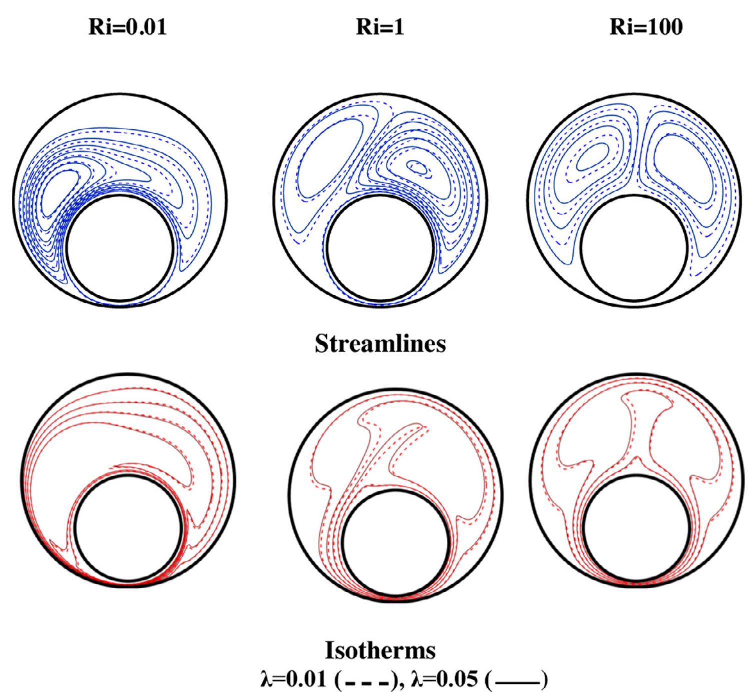

Fig. 6. Streamlines and isotherms for water–TiO2 nanofluid, $\varepsilon = 0.9$.

narrow space below the inner rotating hot cylinder strengthen the external forced convection effect of the rotating inner cylinder. The superposition of these two effects–natural convection in the upper part and forced convection in the lower part–leads to a noticable augmentation in the heat transfer. This augmentation, of course, decreases as the forced convection effect decreases ($1 \leq$ Ri). As the eccentricity decreases, the effect of the forced convection decreases due to the increase in space below the inner cylinder even at small values of Richardson number, this phenomenon is more obvious at $\varepsilon = 0$ (concentric annulus). As the Richardson number increases with decreasing in the eccentricity ($\varepsilon < 0.9$), the natural convection effect is powered, and enhancement in Nusselt number occurs. Fig. 9 represents the augmentation of the average Nusselt number due to the nanoparticles addition for different eccentricities and Richardson numbers. The peak augmentation in the average Nusselt number is established at zero eccentricity (concentric annulus) with mixed convection state (Ri = 1), but the absolute peak average Nusselt number is established at Ri = 0.01 with $\varepsilon = 0.9$, Fig. 8. The effect of nanoparticles addition ($\lambda > 0$) on the convection enhancement is related to the augmentation in the nanofluid thermal conductivity(k_{nf}/k_f), but the temperature gradient at the hot cylinder surface decreases as the thermal diffusivity increases $(k/\rho C_P)_{nf}$. This leads to a decrease or increase in the convection effect relying on the weighting effect ratio between both temperature gradient at the hot cylinder surface and the nanofluid thermal conductivity ratio. Furthermore, the forced convection is powerfully generated at the hot surface (location of the temperature gradient calculation), and any increase in

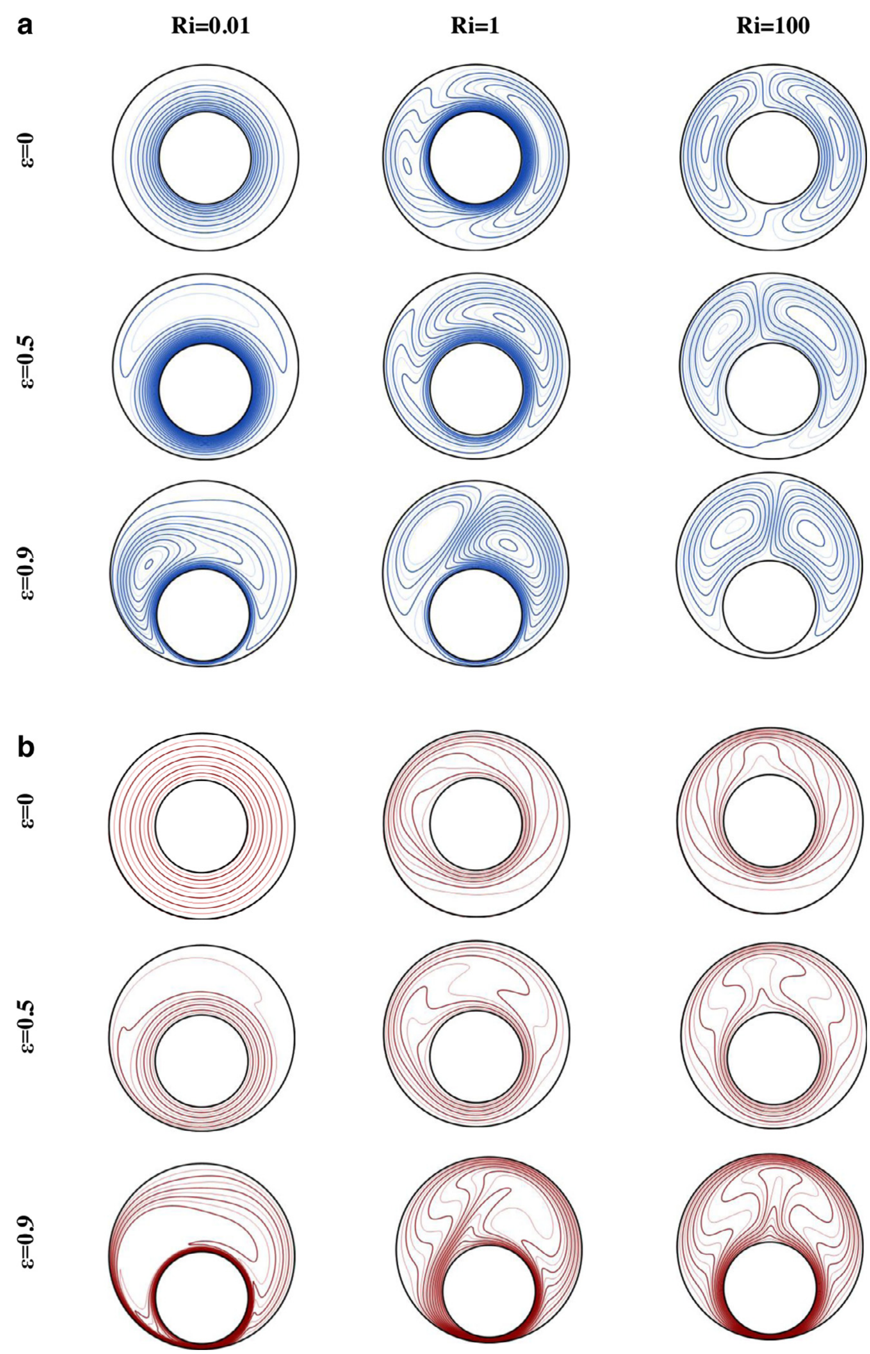

Fig. 7. (a) Streamlines for water–TiO_2 nanofluid, $\lambda = 0.03$. (b) isotherms for water–TiO_2 nanofluid, $\lambda = 0.03$.

the nanoparticles volume fraction leads to an increase in thermal diffusivity. This strengthening in the thermal diffusivity leads to an excessive reduction in the temperature gradient ($\partial\theta/\partial R$) which overcomes the enhancement in the nanofluid thermal conductivity(k_{nf}/k_f). These concepts explain the reported results in Fig. 10. The figure represents the average Nusselt number using different nanofluids (Cu, TiO_2, and Al_2O_3/ water) at different values of Ri and λ with $\varepsilon = 0.9$ as an optimum eccentricity. At Ri = 100, the heat transfer is dominated by the natural convection effect. As the solid volume fraction, λ tends to 0.01, the augmentation in thermal conductivity overcomes the reduction in the temperature gradient and hence peak Nusselt number is established. As the solid volume fraction, λ increases (λ>0.01), the opposite take places. At Ri = 10, the heat transfer is still in the natural convection domain, while the forced convection effect initiates, and the enhancement due to nanoparticles addition is reduced. Moreover, the addition of nanoparticles in natural convection domain (Ri>1) always enhances the heat transfer ($Nu/Nu_{\lambda=0} > 1$) depends on the nanoparticles volume fraction with peak enhancement at $\lambda = 0.01$. At Ri = 1, the effect of the forced convection is more pronounced, and the smaller the nanoparticles volume fraction, the higher the enhancement and vice versa. At both Ri = 0.01 and Ri = 0.1, the forced convection effect is very strong, and the addition of nanoparticles reduces the average Nusselt number.

7.3. Comparison between different nanofluids

A comparison among different types of nanofluids (Cu, TiO_2, and Al_2O_3/ water) is presented in Fig. 10. The results show that,

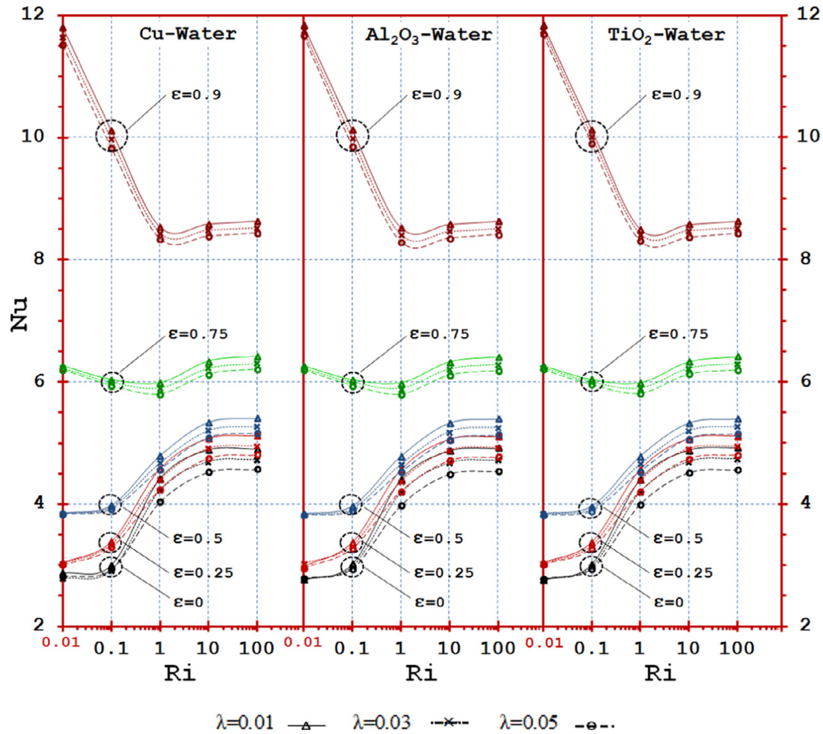

Fig. 8. Average Nusselt Number for different nanoparticle concentrations, and different eccentricities.

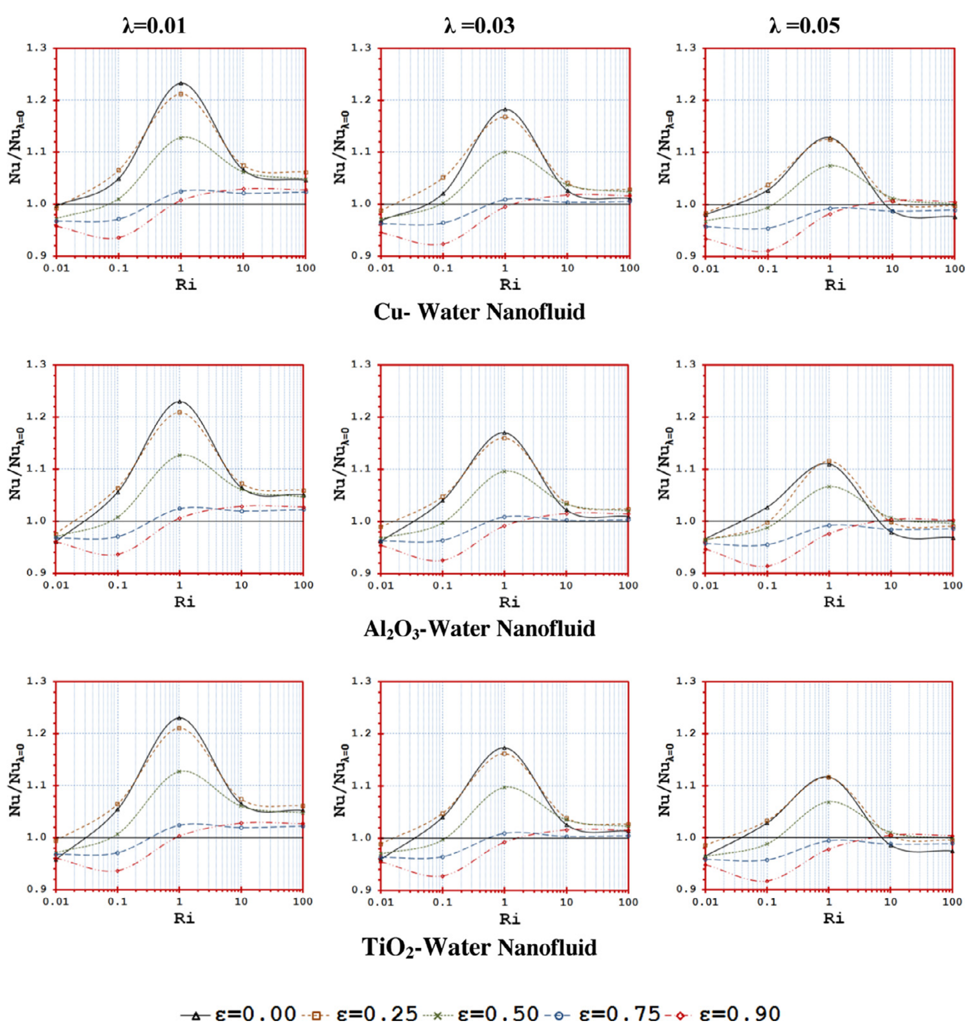

Fig. 9. Average Nusselt Number augmentation due to the nanoparticles addition.

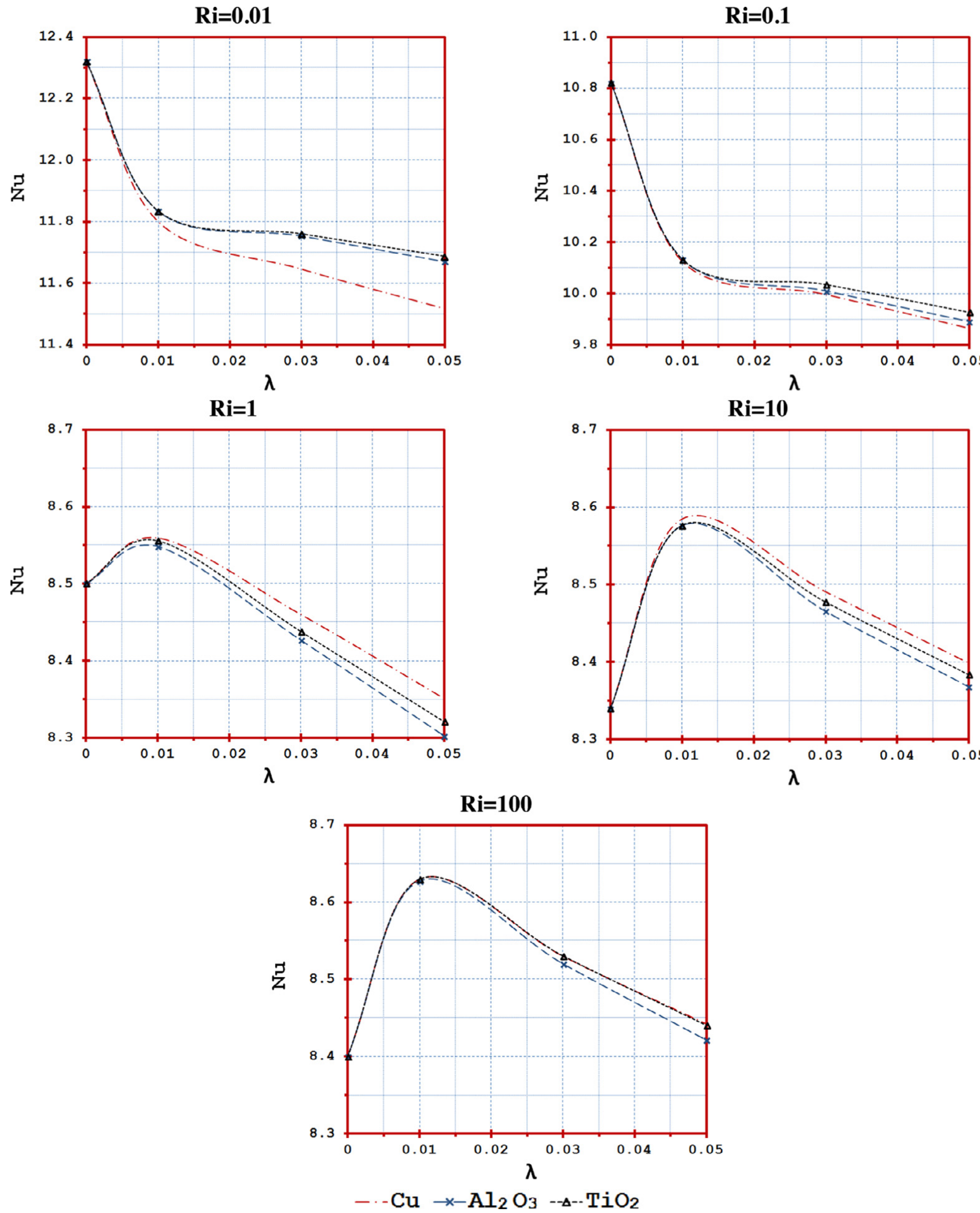

Fig. 10. Average Nusselt number at different concentrations and Richardson numbers, $\varepsilon = 0.9$.

the optimum selection of the nanofluid depends on the heat transfer manner (Ri value). At forced convection domain (Ri = 0.01 and 0.1), it is better to use TiO_2 and Al_2O_3 nanoparticles as an additive to nanofluids for thermal applications. At mixed convection and natural convection heat transfer in the annulus (Ri = 1,10,100), the higher the thermal conductivity, the higher the enhancement of the heat transfer. So, it is better to use Cu nanoparticles ($k = 400$ W/m K) as an additive to nanofluids for thermal applications.

8. Conclusion

In this paper the influence of eccentricity, nanoparticle volume fraction and Richardson number on the average Nusselt number, streamlines and isotherms have been studied for an eccentric annulus filled with (Cu, TiO_2, and Al_2O_3/ water) nanofluids. The optimum and worst operating conditions with respect to the heat transfer are listed in Table 2. The main results could be abbreviated as:

- ➢ The addition of the nanoparticles does not necessarily enhance the heat transfer, the addition of the nanoparticles is related strongly to the Richardson number and the eccentricity ratio.
- ➢ At forced convection heat transfer (Ri = 0.01 and 0.1), the addition of nanoparticles reduces the heat transfer rate particularly at high eccentricity ratio ($\varepsilon = 0.9$) and different nanoparticles type (Cu, TiO_2, and Al_2O_3).
- ➢ The peak augmentation in the heat transfer due to the nanoparticles addition is established at mixed convection manner (Ri = 1) with optimum augmentation at zero eccentricity (concentric annulus).
- ➢ The absolute peak average Nusselt number is established at Ri = 0.01 with $\varepsilon = 0.9$ using regular fluid ($\lambda = 0$).
- ➢ The effect of increasing the nanoparticles solid volume fraction λ has a negative effect on in the domain of forced convection heat transfer (Ri = 0.01 and 0.1), however at mixed convection, Ri = 1, and natural convection, Ri = 10 and 100, it has a positive effect through peak enhancement at $\lambda = 0.01$ for concentric annulus ($\varepsilon = 0$).

Table 2
Optimum and worst operating conditions for heat transfer rate.

			TiO_2–Water				Cu–Water				Al_2O_3–Water			
			λ				λ				λ			
			0	0.01	0.03	0.05	0	0.01	0.03	0.05	0	0.01	0.03	0.05
$Ri = 0.01$	ε	0			×				×				×	
		0.5												
		0.9	√				√				√			
$Ri = 0.1$	ε	0	×				×				×			
		0.5												
		0.9	√				√				√			
$Ri = 1$	ε	0	×				×				×			
		0.5												
		0.9		√				√				√		
$Ri = 10$	ε	0				×				×				×
		0.5												
		0.9		√				√					√	
$Ri = 100$	ε	0				×				×				×
		0.5												
		0.9		√				√					√	

Note: The mark (√) refers to optimum and (×) for worst.

References

[1] Date AW. Numerical prediction of natural convection heat transfer in horizontal annulus. Int J Heat Mass Transf 1986;29:1457–64.
[2] Ho CJ, Lin YH. Laminar natural convection of cold water enclosed in a horizontal annulus with mixed boundary conditions. Int J Heat Mass Transf 1988;31:2113–21.
[3] Ho CJ, Lin YH. Natural convection in a horizontal annulus partially filled with cold water. Int J Heat Mass Transf 1991;34:1371–82.
[4] Ho CJ, Lin YH, Chen TC. A numerical study of natural convection in concentric and eccentric horizontal cylindrical annuli with mixed boundary conditions. Int J Heat Fluid Flow 1989;10:40–7.
[5] Kumar R. Study of natural convection in horizontal annuli. Int J Heat Mass Transf 1988;31:1137–48.
[6] McLeod AE, Bishop EH. Turbulent natural convection of gases in horizontal cylindrical annuli at cryogenic temperatures. Int J Heat Mass Transf 1989;32:1967–78.
[7] Yan-Fei R, Yasutomi M, Kenji F, Yasuyuki T, Shu H. Flow patterns of natural convection in horizontal cylindrical annuli. Int J Heat Mass Transf 1985;28:705–14.
[8] Sambamurthy NB, Shaija A, Narasimham GSVL, Murthy MVK. Laminar conjugate natural convection in horizontal annuli. Int J Heat Fluid Flow 2008;29:1347–59.
[9] Yoo J-S. Natural convection in a narrow horizontal cylindrical annulus: $Pr \leq 0.3$. Int J Heat Mass Transf 1998;41:3055–73.
[10] Yoo J-S. Prandtl number effect on bifurcation and dual solutions in natural convection in a horizontal annulus. Int J Heat Mass Transf 1999;42:3279–3290.
[11] Yoo J-S. Transition and multiplicity of flows in natural convection in a narrow horizontal cylindrical annulus: $Pr = 0.4$. Int J Heat Mass Transf 1999;42:709–22.
[12] Adachi T, Imai S. Three-dimensional linear stability of natural convection in horizontal concentric annuli. Int J Heat Mass Transf 2007;50:1388–96.
[13] Hu Y, Li D, Shu S, Niu X. Study of multiple steady solutions for the 2D natural convection in a concentric horizontal annulus with a constant heat flux wall using immersed boundary-lattice Boltzmann method. Int J Heat Mass Transf 2015;81:591–601.
[14] Luo K, Yi H-L, Tan H-P. Eccentricity effect on bifurcation and dual solutions in transient natural convection in a horizontal annulus. Int J Therm Sci 2015;89:283–93.
[15] Mizushima J, Hayashi S, Adachi T. Transitions of natural convection in a horizontal annulus. Int J Heat Mass Transf 2001;44:1249–57.
[16] Petrone G, Chénier E, Lauriat G. Three-dimensional study of multiple transitions for natural convection in horizontal annuli. Int J Heat Mass Transf 2006;49:1231–41.
[17] Aldoss TK, Alkam M, Shatarah M. Natural convection from a horizontal annulus partially filled with porous medium. Int Commun Heat Mass Transf 2004;31:441–52.
[18] Khanafer K, Al-Amiri A, Pop I. Numerical analysis of natural convection heat transfer in a horizontal annulus partially filled with a fluid-saturated porous substrate. Int J Heat Mass Transf 2008;51:1613–27.
[19] Kumari M, Nath G. Unsteady natural convection from a horizontal annulus filled with a porous medium. Int J Heat Mass Transf 2008;51:5001–7.
[20] Lai FC. Natural convection in a horizontal porous annulus with mixed type of radial baffles. Int Commun Heat Mass Transf 1993;20:347–59.
[21] Mota JPB, Esteves IAAC, Portugal CAM, Esperança JMSS, Saatdjian E. Natural convection heat transfer in horizontal eccentric elliptic annuli containing saturated porous media. Int J Heat Mass Transf 2000;43:4367–79.
[22] Sen M, Torrance KE. Natural convection in a thin horizontal porous annulus. Int J Heat Mass Transf 1987;30:729–39.
[23] EJM E, S KS, M S, A N, R KS. Cerium oxide–ethylene glycol nanofluids with improved transport properties: preparation and elucidation of mechanism. J Taiwan Inst Chem Eng 2015;49:183–91.
[24] Meybodi MK, Daryasafar A, Koochi MM, Moghadasi J, Meybodi RB, Ghahfarokhi AK. A novel correlation approach for viscosity prediction of water based nanofluids of Al2O3, TiO2, SiO2 and CuO. J Taiwan Inst Chem Eng 2016;58:19–27.
[25] Shanbedi M, Heris SZ, Amiri A, Eshghi H. Synthesis of water-soluble Fe-decorated multi-walled carbon nanotubes: a study on thermo-physical properties of ferromagnetic nanofluid. J Taiwan Inst Chem Eng 2016 In Press.
[26] Su F, Ma X, Lan Z. The effect of carbon nanotubes on the physical properties of a binary nanofluid. J Taiwan Inst Chem Eng 2011;42:252–7.
[27] Alawi OA, Sidik NAC, Dawood HK. Natural convection heat transfer in horizontal concentric annulus between outer cylinder and inner flat tube using nanofluid. Int Commun Heat Mass Transf 2014;57:65–71.
[28] Ashorynejad HR, Mohamad AA, Sheikholeslami M. Magnetic field effects on natural convection flow of a nanofluid in a horizontal cylindrical annulus using Lattice Boltzmann method. Int J Therm Sci 2013;64:240–50.
[29] Mehrizi AA, Farhadi M, Shayamehr S. Natural convection flow of Cu–Water nanofluid in horizontal cylindrical annuli with inner triangular cylinder using lattice Boltzmann method. Int Commun Heat Mass Transf 2013;44:147–56.
[30] Yu Z-T, Xu X, Hu Y-C, Fan L-W, Cen K-F. A numerical investigation of transient natural convection heat transfer of aqueous nanofluids in a horizontal concentric annulus. Int J Heat Mass Transf 2012;55:1141–8.
[31] Abu-Nada E, Masoud Z, Hijazi A. Natural convection heat transfer enhancement in horizontal concentric annuli using nanofluids. Int Commun Heat Mass Transf 2008;35:657–65.
[32] Habibi Matin M, Pop I. Natural convection flow and heat transfer in an eccentric annulus filled by Copper nanofluid. Int J Heat Mass Transf 2013;61:353–364.
[33] Al-Amiri AM, Khanafer KM. Numerical simulation of double-diffusive mixed convection within a rotating horizontal annulus. Int J Therm Sci 2006;45:567–78.
[34] Teamah MA. Numerical simulation of double diffusive laminar mixed convection in a horizontal annulus with hot, solutal and rotating inner cylinder. Int J Therm Sci 2007;46:637–48.
[35] Mozayyeni HR, Rahimi AB. Mixed convection in cylindrical annulus with rotating outer cylinder and constant magnetic field with an effect in the radial direction. Sci Iran 2012;19:91–105.
[36] Char M-I, Hsu Y-H. Numerical prediction of turbulent mixed convection in a concentric horizontal rotating annulus with low-Re two-equation models. Int J Heat Mass Transf 1998;41:1633–43.
[37] Khanafer K, Chamkha AJ. Mixed convection within a porous heat generating horizontal annulus. Int J Heat Mass Transf 2003;46:1725–35.
[38] Cao Z-H, Luo K, Yi H-L, Tan H-P. Energy conservative dissipative particle dynamics simulation of mixed convection in eccentric annulus. Int J Heat Mass Transf 2014;74:60–76.
[39] Lee TS. Numerical computation of fluid convection with air enclosed between the annuli of eccentric heated horizontal rotating cylinders. Comput Fluids 1992;21:355–68.
[40] Patankar SV. Numerical Heat Transfer and Fluid Flow. New York: McGraw-Hill; 1980.

[41] El-Maghlany WM, Saqr KM, Teamah MA. Numerical simulations of the effect of an isotropic heat field on the entropy generation due to natural convection in a square cavity. Energy Convers Manag 2014;85:333–42.
[42] Teamah MA, El-Maghlany WM. Numerical simulation of double-diffusive mixed convective flow in rectangular enclosure with insulated moving lid. Int J Therm Sci 2010;49:1625–38.
[43] Teamah MA, El-Maghlany WM. Augmentation of natural convective heat transfer in square cavity by utilizing nanofluids in the presence of magnetic field and uniform heat generation/absorption. Int J Therm Sci 2012;58:130–42.
[44] Maxwell JCA. Treatise on Electricity and Magnetism. 3rd ed. New York: Dover; 1954.
[45] Koo J, Kleinstreuer C. Laminar nanofluid in micro heat-sinks. Int J Heat Mass Transf 2005;48:2652–61.
[46] Brinkman HC. The viscosity of concentrated suspensions and solution. J Chem Phys 1952;20:571–81.
[47] Sheikholeslami M, Ganji DD. Nanofluid flow and heat transfer between parallel plates considering Brownian motion using DTM. Comput Methods Appl Mech Eng 2015;283:651–63.